Senior Thesis

Ultrafast Dynamics of a Molecular Rotor and Applications to Biological Systems

Ian A. Nilsen

Department of Chemistry, University of Michigan, 930 N. University Ave., Ann Arbor, MI 48109

Email: inilsen@umich.edu

Table of Contents

Chapter 1. Abstract and Introduction

1.1: Abstract

The structure and properties of benzene chromium tricarbonyl ($C_6H_6Cr(CO)_3$, BCT) were studied using infrared spectroscopy. BCT was found to undergo torsional motion about the arene-metal bond with a barrier roughly half of k_BT and the reaction coordinate was mapped using density functional theory (DFT). Using ultrafast two-dimensional infrared spectroscopy, the torsional motion was found to occur on a ~3ps timescale and was independent of solvent viscosity. The metal-carbonyl bond of BCT can be dissociated using a broadband UV source; geminate rebinding measurements provide the ability to determine the conformation of BCT complexed with β-cyclodextrin. It was determined that there are two complexes: one with the carbonyl ligands pointing out of the hydrophobic cavity and one with them pointing into the cavity. BCT was then complexed to cholesterol in an attempt to study the constrained water environment in reverse micelles. Due to the lack of charge attraction between BCT and the micelle head groups, localization at the water-micelle interface was difficult to accomplish; to combat this sodium thiocyanate was used in studies of micelles as well and was found to be localized inside the polar water cavity.

1.2: Introduction

Spectroscopy is a powerful tool for understanding the underlying interactions of atoms and molecules. From early-20th century experiments, the duality of light as both a particle and a wave allowed for the enhanced understanding of light-matter interactions using quantum mechanics. Depending on the energy of a photon, which is proportional to its frequency, a variety of different outcomes can occur depending on the composition of the target atom, molecule, or cluster. In general, the field will interact with the target in some way, either transferring energy (absorption), or deflecting its path (scattering). For spectroscopy, the focus is on the transfer of energy from a photon causing a molecule to enter excited states.

Molecules contain a number of rotational, vibrational, and electronic energy levels that can be accessed with enough energy from an incident photon. A "ground" or lowest energy level is most commonly populated at room temperature and the distribution of the energy level population is characterized through a Boltzmann distribution. To excite a molecule to a higher electronic, vibrational, or rotational state, the field must match the energy difference of the two modes and have a nonzero transition moment. Thus, microwave radiation may be used to excite rotational modes, infrared radiation is used to excite vibrational states, and ultraviolet as well as visible radiation is used to excite electronic transitions.

Vibrational spectroscopy has a number of common uses, including functional group determination for synthesis applications. Atoms have different masses, and treating vibrations using a harmonic oscillator model allows fairly accurate determination of the appropriate vibrational frequencies. Another important, but more subtle application of infrared spectroscopy is the effect of environment on the vibrational frequency and line width. For instance, in general a vibrational mode will broaden in more polar solvents compared to apolar solvents as the

fluctuating solvent molecules create a changing electric field that affects the motion of the atoms. These sorts of effects can be observed in linear IR spectra, but for equilibrium studies and ultrafast reaction kinetics, the nuances of molecular motion are often lost as the linear technique only measures what energy was absorbed, not how the energy evolves with time. For this sort of measurement, another dimension needs to be added so that the frequency detected can be correlated with the frequency excited. One shortcoming of absorptive infrared measurements is that signal intensity and elevation above background noise are low due to the longer time averaging takes compared to interferometry-based methods, so only strong vibrational modes can be accurately distinguished from the background.

The location of metal carbonyl vibrational stretches in the "clear window" (1850-2100 cm^{-1}) of the infrared spectrum, free of interference from common spectral contaminants such as carbon dioxide and water vapor, makes them suitable as probes of complex environments. These compounds are ideally suited to 2D-IR spectroscopy, a method in third-order nonlinear spectroscopy that gives information about how two vibrational frequencies are correlated. Metal carbonyl containing compounds have shown promise bound to proteins to probe solvent dynamics at the solvent-protein interface[1]. They have also been useful understanding isomerization pathways that occur on picosecond timescales[2,3].

Piano-stool compounds represent an interesting class of simple metal carbonyl compounds and have been well studied due to their overall structural simplicity. One interest of past researchers is the ability of some piano-stool complexes to undergo torsional motion around an arene-metal bond[4,5]. With recent advances in nanotechnology and engineering, it has proved possible to create synthetic molecular rotors that exhibit unidirectional motion, provided there is some external driving force[6,7]. Ultrafast fluorescence suggests that optical control of the excited

state can be used to modulate unidirectional torsional motion of light-activated molecular rotors, providing an interesting way to provide the equivalent of a "power-stroke" as seen in conventional engines. However, while the processes required to drive a rotor in one direction have been well characterized, the equilibrium interactions of the rotor and solvent have not been nearly as well studied. The laws of thermodynamics dictate unidirectional motion at equilibrium is unachievable[8]. In contrast with typical macroscopic machines, designing a nano-machine requires understanding both the active interactions driving the unidirectional motion and the passive interactions between the machine and the surrounding environment. The latter can be studied under equilibrium conditions, providing insight into the effect microscopic friction can have on a synthetic rotor.

Benzene chromium tricarbonyl ($C_6H_6Cr(CO)_3$, BCT, **Fig. 1**) is a particularly intriguing piano-stool compound as it has been found to undergo torsional motion[9], and the benzene ring can be functionalized to study biological systems. Complexation of BCT with β-cyclodextrin, which contains a relatively hydrophobic cavity compared to the aqueous environment, provides a good model for molecular recognition. Functionalizing the benzene ring with an acidic group allows the probe to attach to biologically relevant molecules like cholesterol, which can be incorporated into larger systems such as micelles or proteins with the hope of studying constrained water. The solvent interaction with large biomolecules often relies upon the hypothesis that water near membranes behaves differently than bulk water[10]. Reverse-micelles with a polar core and a nonpolar exterior provide an opportunity to study constrained water dynamics at the micelle interface in a very controlled environment.

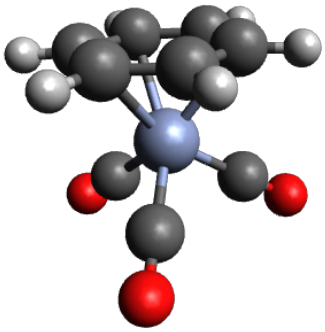

Figure 1: A 3D ball and stick model of BCT.

The aim of this work is to investigate the properties of BCT and their applicability to ultrafast spectroscopy of complex chemical and biological systems. Using ultrafast 2D-IR spectroscopy, we can observe molecular dynamics at femtosecond timescales providing information on the fastest motions molecules undergo. First, the internal torsional reaction coordinate of BCT will be discussed within the framework of ultrafast spectroscopy and kinetics. Second, BCT will be attached to a variety of molecules in an effort to study constrained solvent dynamics in biological systems.

Chapter 2. Methods and Theoretical Background

2.1: BCT Complexation with Cyclodextrin and Side-chain Modification

BCT and β-CD were purchased from Sigma Aldrich and were used without further purification, as were all solvents including those used in filtration steps. The procedure for creation of the host-guest inclusion complex was modified from a similar procedure for cyclopentadienyl manganese tricarbonyl (CMT)[11]. BCT was ground from factory crystals to a fine powder, and then combined with β-CD in water at 60ºC for 2 hours. The inclusion complex is virtually insoluble in water, and can be vacuum filtered out of the reaction mixture. A light yellow powder was obtained following a wash with water and benzene to remove unreacted BCT and β-CD. BCT with a carboxylic acid functionalized benzene ring was purchased from Sigma Aldrich and used in a Steglich esterification procedure to form ester linkages to alcohols such as glycerol and cholesterol for use in micelle studies.

2.2: Reverse Micelle Creation and Methods for Inclusion

Reverse micelles with a polar water cavity were created with both negatively charged head groups (dioctyl sodium sulfosuccinate, AOT) and positively charged head groups

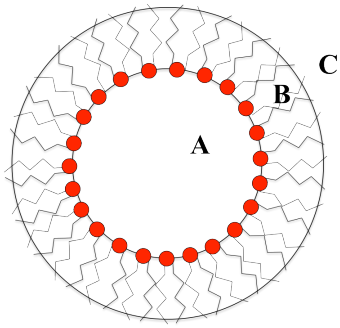

Figure 2: Schematic diagram of a micelle showing the polar water core (A), the micelle interface (B), and the organic bulk phase (C). The red micelle head group is typically charged.

(ammonium bromide). A schematic of a reverse micelle and the zones for a guest molecule to reside are shown in **Fig. 2**. Three different chain length ammonium bromide molecules were used to give differing cavity radii: cetrimonium bromide (CTAB), tetradecyltrimethylammonium bromide (TTAB), and dodecyltrimethylammonium bromide (DTAB). AOT was purified using a literature protocol[12]; the ammonium bromide molecules were used as received from Sigma Aldrich.

For AOT micelles, the size of the micelle has been found to vary with parameter w_0, defined as:

$$w_0 = \frac{[water]}{[AOT]} \quad (1)$$

The ratio of w_0 can be varied to give different size cavity reverse micelles. A procedure similar to the literature was used for formation of micelles[12], where a 50mM solution of AOT in isooctane was vortex mixed, sonicated, and stirred before addition of the BCT side chain derivative dissolved in water. The size of AOT micelles was determined using an ALV Dynamic Light Scattering (DLS) apparatus with a Coherent Innova 70C laser as the light source centered at 498 nm. DLS is a technique that measures the size of the particles based on the Rayleigh scattering of the light, for this experiment the scattering angle for detection was set to 90º and 60º with consistent results for the radius of the micelles.

The ammonium bromide reverse micelles were prepared similarly, in accordance with a past literature method[13], with the exception that isooctane was used instead of hexane and hexanol was used as the stabilizing agent. Because the presence of the stabilizing agent could affect the spectra and lead to preferential solvation effects, for the ammonium bromide series of micelles dichloromethane (DCM) dissolves the lipids and creates stable phases without a co-solvent so it was used instead of the isooctane. As with the AOT reverse micelles, the water added (w_0 = 4) to form the polar core contained the BCT side chain derivative. Due to the fact

that ammonium bromide groups are positively charged, a negatively charged probe (sodium thiocyanate, NaSCN) was used as well to see if electrostatic attraction caused better inclusion of the probe in the water cavity as opposed to being in the bulk nonpolar phase.

2.3: Fourier-transform Infrared Spectroscopy

Fourier-transform infrared spectroscopy (FTIR) was utilized to characterize the vibrational modes of BCT before any two-dimensional studies could be undertaken. In addition, the characteristic vibrational modes of a particular molecule shift depending on their environment; in many cases this can be easily seen with an FTIR. The downfall of FTIR is the inability to time-resolve any shifts in the spectrum that occur faster than a few seconds. Worse still is that one lacks an ability to decouple homogeneous and inhomogeneous broadening, so any hypothesis explaining the changing line width is possible. To obtain information about the underlying processes causing the change in line shape, multi-dimensional spectroscopy must be used and is explained in more detail in the following section. Thus, fast chemical exchange and molecular reorientation appear purely as average states in an FTIR spectrum and the individual species are unresolvable.

FTIR spectra were taken using a Jasco FTIR-4100 spectrometer. Sample cells consisted of a 100μm Teflon spacer placed between two 3mm thick calcium fluoride windows. A background scan of the matrix was used as a blank to allow for easier differentiation from the sample. It is important for accurate measurement of the properties of a molecule in solution that it be in as homogenous a phase as possible. To that end, samples were vortex mixed and sonicated in order to promote mixing. In addition, samples of BCT and BCT complexes were prepared at low concentrations, near 5 mM to avoid any potential aggregation effects. Micelles studied using FTIR were prepared to as large a concentration as was able to be solvated due to a

need to overcome the low optical density. This low optical density stems from the fact that relative to BCT and other tricarbonyl probes; micelles are fairly large and have a tendency to scatter light. Linear alkane and alcohol solvents were used as received, with no further purification. FTIR spectra were exported as ASCII files and analyzed using MATLAB09 to normalize the series of spectra by area. For photodissociation studies of the carbonyls, a broadband UV lamp was mounted on an O-ring and positioned so it constantly irradiated the FTIR sample and measurements were made every few seconds.

2.4: 2D-IR Spectroscopy

2D-IR is a method in third-order nonlinear spectroscopy; so named because of the three field interactions with the sample (**Fig. 3**) required for the experiment and the usage of nonlinear optical processes to manipulate the frequency of the light. The method is used for correlating the excited frequency with where the energy from that vibrational mode evolves to (detected frequency), as a function of time. The method allows for the resolution of states that could be inhomogenously broadening the linear spectrum and allows for time resolution of interconversion between these states. Inhomogeneous broadening results from the different available microstates that have slightly different individual vibrational modes. When many vibrational microstates are sampled, we obtain a vibrational mode that has a characteristic width corresponding to the number of states sampled. For instance, water molecules do not have constant length hydrogen bonds; rather, the bond lengths vary and the slightly differing

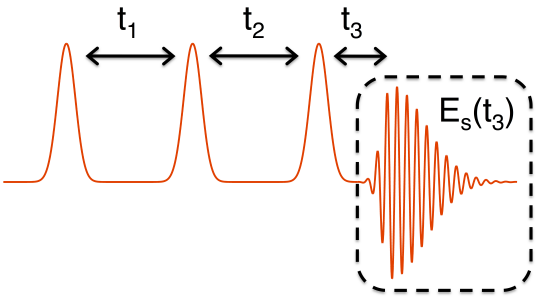

Figure 3: The pulse sequence diagram for 2DIR experiments.

environments affect the electron density, in turn affecting the vibrational frequency. A 1D infrared spectrum cannot tell you, in principle, if an inhomogeneously broadened band spectrally diffuses or not, nor is the method fast enough to provide any time resolution even if it could. While it is possible in some cases to make predictions about the 2D spectra from the line shape[14] of the linear FTIR spectra, the models lose some dynamical information that may only be gained from a 2DIR spectrum. Time resolution in the femtosecond and picosecond range allows for experimenters to follow reactions on ultrafast timescales, allowing for resolution of solvent reorganization and rapidly isomerizing molecules[1,15].

The procedure for 2DIR experiments conducted in the Kubarych lab has been described in detail[16]. Briefly, 2DIR involves excitation of a sample into a vibrational coherence with an infrared pulse signified by t_1, then into a vibrational population with a second pulse. After a period called the waiting time and signified by t_2, a third pulse puts the sample back into a vibrational coherence and it is detected as ω_3, or the detected frequency. The t_1 coherence time is Fourier transformed into the frequency domain, yielding the excited frequency ω_1. During the t_2 time depending on the nature of the system either spectral diffusion or chemical exchange can occur and are discussed below. The infrared pulses are generated from a Ti:sapphire laser, centered at 800 nm with a 1 kHz repetition rate. In order to generate IR pulses, the beams are passed through a birefringent crystal of β-barium borate (BBO) in a dual optical parametric amplifier (OPA) followed by difference-frequency generation in separate GaSe crystals. The first beam is split, forming the first two pulses, and the beams are arranged in a box geometry, which then all converge at the sample generating the signal. The signal and reference local oscillator are upconverted by sum-frequency generation into the visible region in order to make detection easier, capable of detection by a standard 1340 x 100 pixel silicon CCD. This allows for the

detection of the entire infrared region without the need for a much more expensive infrared detector.

During the t_2 waiting time, the vibrationally excited system evolves. There are two major regimes that are often applicable: spectral diffusion and chemical exchange. Both regimes are used to describe the vibrational transfer from an excited mode to a detected one. In the case of chemical exchange, the two species of interest are separated enough to clearly be resolvable as two spectral bands (**Fig. 4**). At short waiting times, the frequency detected is strongly correlated to the frequency excited, as not enough time has passed for the system to evolve. However, as t_2 increases, the spectra begin to show cross-peaks that appear due to the interconversion between the species. One commonly used method for quantitating the chemical exchange rate is by integrating the area of the cross-peaks as a function of time and fitting the resulting curve to get a time constant.

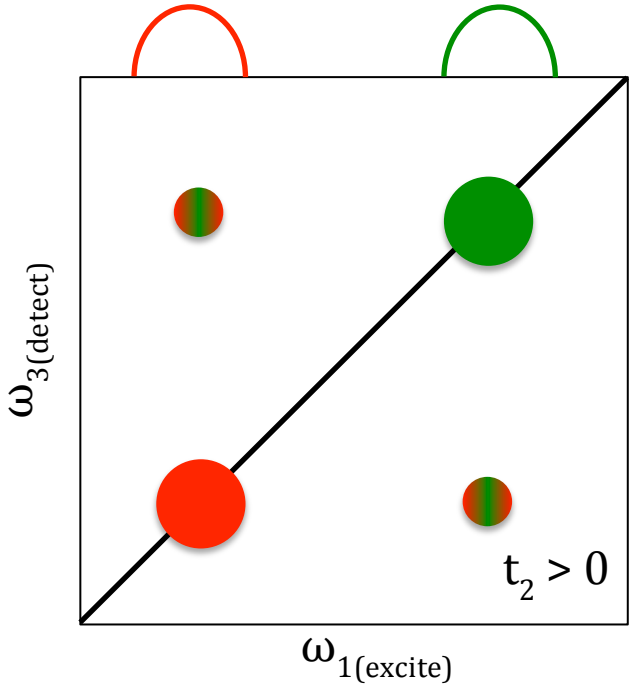

Figure 4: A typical chemical exchange experiment has both correlated diagonal peaks and clearly resolved off-diagonal cross peaks, which correspond to vibrational energy transfer between the two distinct chemical species. Fitting the cross peak volume as a function of t_2 time gives insight into the timescale for chemical exchange.

In contrast, spectral diffusion refers to the inhomogeneous broadening of a band due to different microstates, such as the water hydrogen-bonding example. Spectral diffusion measurements have been useful for quantitative insight into the mobility of solvent molecules in the bulk versus constrained near the surface of a protein or other large molecule. In general, the spectral diffusion timescale is the amount of time for one microstate to sample all the others that broaden the band of interest. As a molecule samples the other available microstates, the strongly correlated peak along the diagonal broadens until the correlation is lost (**Fig. 5**).

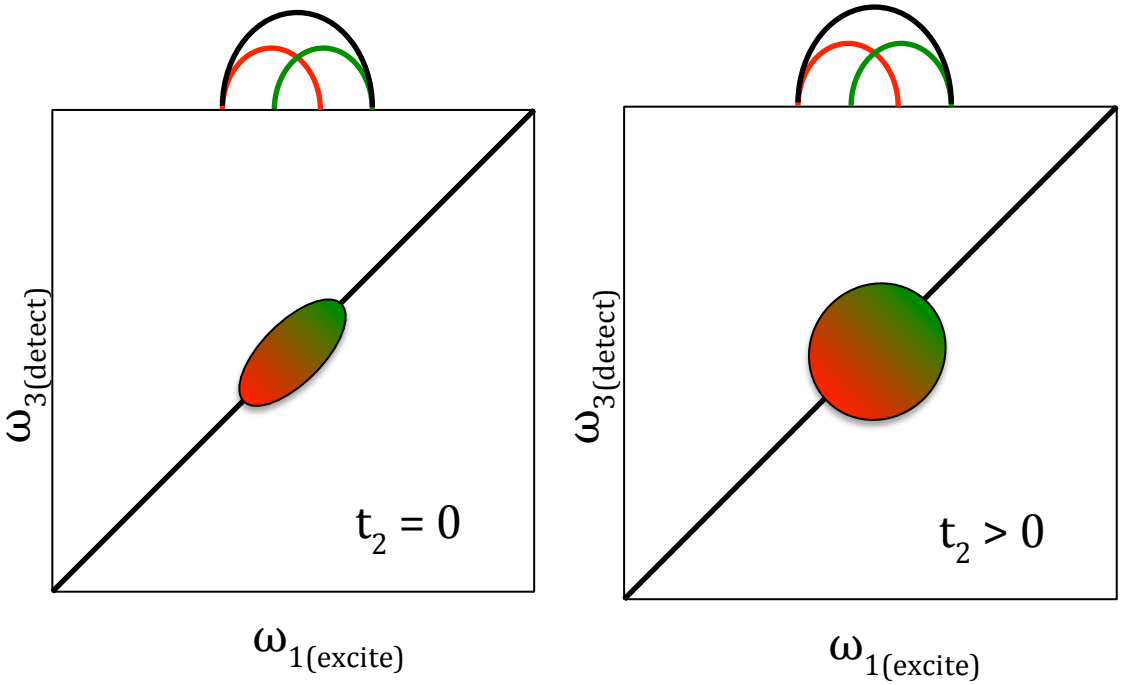

Figure 5: A typical spectral diffusion measurement involves observing the loss of correlation in the excited and detection frequencies as a function of waiting time; this can be seen in a "broadening" of the 2D spectrum.

A general way to differentiate chemical exchange and spectral diffusion is that in spectral diffusion there are usually not distinct chemically different isomers that could potentially be isolated. There are a number of ways to measure the spectral diffusion, such as the centerline slope method[17] and 2DIR cross-peak volume method[18], but for some simple cases, such as the

BCT internal torsional reaction coordinate, a method developed in the Kubarych Lab called the "Rapidly Acquired Spectral Diffusion" or RASD method may be used[19].

2.5: The Frequency-Frequency Correlation Function and RASD Method

When multiple conformations are available to a molecule, each inducing fluctuations in the vibrational frequency, as discussed previously we observe a broadening in the linear FTIR spectrum. The temporal correlation of these vibrational frequency fluctuations is known as the frequency fluctuation correlation function (FFCF). The FFCF is commonly modeled as:

$$\langle \delta\omega(t)\delta\omega(0)\rangle = \frac{\delta(t)}{T_2} + \sum_i \Delta_i^2 exp\left(\frac{-t}{\tau_i}\right) \qquad (2)$$

Where $\delta\omega(t)$ is the frequency fluctuations away from the mean, $\delta(t)$ is the delta function, t_2 is the pure-dephasing time, Δ_i is the amplitude of the frequency fluctuations, and τ_i is the spectral diffusion time constant. The FFCF can be used to fit the experimental data for spectral diffusion and determine the spectral diffusion time.

For the BCT internal torsional reaction coordinate, the energy difference between the two isomers broadening the symmetric stretch was found to be a very small 2 cm^{-1}. Typically, this system would be thought about as a chemical exchange problem due to the presence of structurally different isomers. However, the low barrier allows us to think of the problem as a spectral diffusion problem with only one peak broadening as BCT rotates under equilibrium conditions. This simplifies the system down to one similar to that shown in the idealized case for spectral diffusion in **Fig. 5**.

The experimental setup and data acquisition for the RASD method uses the same setup described earlier for full 2DIR experiments. Previously, the ability to measure the FFCF from 2DIR spectra was studied utilizing the inhomogeneous index[20]:

$$I.I. = \frac{A_r - A_n}{A_r + A_n} \quad (3)$$

Where A_r and A_n represent the rephasing and nonrephasing peak volumes, respectively, of the mode of interest. The difference between rephrasing and nonrephasing spectra stems from the orientation of the wave vectors of the pulses, $\mathbf{k_R = -k_1 + k_2 + k_3}$ and $\mathbf{k_N = +k_1 - k_2 + k_3}$. The difference in orientation shows up in the generation of cross-peaks; a more complete discussion of the effects of rephrasing and nonrephasing spectra and their importance in 2DIR may be found in a comprehensive review by Ogilvie & Kubarych[21]. Here, we utilize the inhomogeneous index rather than the 2DIR peak volume, A_r and A_n represent the amplitudes of the t_1 resolved heterodyne detected signal. Under the short time approximation, the rapidly acquired spectral diffusion (RASD) is represented as:

$$RASD = \text{erf}\left(t_1 \bar{C}(t_2) \sqrt{\frac{\langle \delta\omega^2 \rangle}{2}}\right) \quad (4)$$

Where $\bar{C}$ is the normalized correlation function. It should be noted that the magnitude of t_1 acts as a scaling factor and is selected to maximize the signal to noise ratio. The exact setting of the t_1 time only serves to scale the FFCF; it does not affect the decay, which is where the spectral diffusion time constant is extracted.

2.6: Quantum Chemistry Calculations

Density functional theory (DFT) is a useful tool for approximating the energy states of BCT along the reaction coordinate due a couple of factors. First, because only the first and second order density matrices are needed, the number of coordinates reduces from 3N to 6 saving a large amount of computational time compared to more expensive methods. Second, when looking at

the torsional reaction coordinate the principle concern is the relative energies, not the absolute energies, so any systemic error from the approximations used in the method should cancel out. The calculations were performed in GAUSSIAN03[22] using the B3LYP functional for geometry optimizations and BP86 for frequency calculations with the 6-311+G(d,p) basis set for the carbon, oxygen and hydrogen atoms. The optimized structures from B3LYP were reoptimized using BP86 before the frequency calculation was run, because in general different functionals optimize the structure slightly differently which could lead to frequencies that are not meaningful. The LANL2DZ basis set and pseudopotential was used for the chromium atom to account for the added electron density; this is consistent with modeling approaches for other metal carbonyl structures[3]. The choice of basis and functional is consistent with a past study for hexacarbonylchromium, which showed B3LYP and BP86 give similar results for geometry optimizations; however, BP86 tends to optimize vibrational frequencies closer to the experimental values[23]. The optimized structures not located at saddle points on the potential energy surface were calculated by constraining the dihedral angles between the carbonyls and the benzene ring while optimizing the geometry with respect to the other degrees of freedom. The coordinates for optimized geometry structures for the staggered and eclipsed states may be found in Chapter 6. Frequency calculations were done on the stable isomers, but due to limitations in the computational method, frequency calculations of non-minima or saddle points for this molecule are not meaningful. Molecular volumes of the BCT stable states were also computed. To test the solvent dependence of the torsional coordinate frequency of BCT, calculations implementing a polarizable continuum model (PCM) were performed using built in solvent models of n-hexane, n-nonane, n-dodecane, and n-pentane. PCM calculations were performed using GAUSSIAN09[24].

2.7: Modeling Strategies: Classical Langevin Simulations and Kinetic Studies

When doing a 2DIR experiment, it is commonly assumed that the decay in the frequency fluctuation correlation function can be fit to a single exponential, thus giving a time constant for the frequency flux. However, understanding the timescale of reactions is what is most interesting, for which the FFCF is only a proxy measurement that needs to be mapped onto the reaction coordinate. Often, there are a variety of competitive processes that can lead to more complicated frequency fluctuation correlation functions. Elucidating the underlying reactions from the data can be difficult; one strategy is directly attempting to model the motion and linking it to the frequencies observed from the experiments. Another strategy involves looking at the competing rates between stable energy states using chemical kinetics. The difficulty with kinetics is that in many cases simplifying assumptions are difficult to make and the rates obtained from solving differential equations are not meaningful. With BCT however, it is easy to imagine six equivalent potential wells due to the periodic nature of the potential; then solving the differential equations yields the timescale it takes a population starting in one well to move to all the other wells.

BCT torsional motion can be modeled using a 1-D Langevin simulation[25]. From quantum chemistry calculations using density functional theory, it was found that the benzene ring rotates with respect to the $Cr(CO)_3$ portion. The reaction occurs on a single angular coordinate, which allows for treatment with a 1-D angular Langevin simulation. The total torque on a particle at time *t* is given by:

$$\tau(t) = -\zeta\dot{\theta}(t) - \frac{\partial V}{\partial \theta} + A(t) \qquad (5)$$

The first term represents the friction opposing the angular velocity. The energy values from the quantum chemistry calculations using DFT were used to generate a periodic potential energy

curve V(θ), which can be differentiated to provide the force. The random fluctuating torque A(t) was generated using a Gaussian white noise distribution and the friction was linked to viscosity using a modified form of the Stokes-Einstein relationship used in similar simulations[26]:

$$\zeta = 8\pi\eta r^3 c_{slip}$$

Physical quantities, such as the moment of inertia, were calculated assuming a stationary $Cr(CO)_3$ portion and rotating benzene ring. The slip-stick coefficient was set to a value of 1, implying full stick conditions[26]. Each simulation was run for 80 ns, with 1 fs step size. The initial position of the particle was randomly selected, then allowed to equilibrate for a short period of time before the simulation began. Due to the symmetry of the reaction coordinate, periodic boundary conditions were used in order to simplify the simulation. The angular trajectories then were converted to frequencies using the results of the DFT frequency calculations. The change in frequency between the two energy wells was small enough that assuming the frequency, as a function of the angular coordinate, was directly proportional to the potential energy surface proved sufficient. A critical assumption of the classical simulation is that the viscosity, which is linked to the friction, directly correlates with the timescale of the motion of the rotor. It will be seen from the 2DIR measurements that this is not the case for the BCT internal torsional coordinates and the classical Langevin model does not apply. However, it is included in this work in the event future studies of rotors do follow the trend with viscosity, which is possible in a number of scenarios, such as larger functional groups than protons being attached to the arene ring.

Brownian motion of a particle in a periodic potential has been described previously[27]; due to the finite periodic nature of the potential, the BCT internal reaction coordinate is amenable to multi-state kinetics. Based on the symmetry of the molecule, there are six identical global

minima corresponding to each staggered conformation. Using a six-state kinetic model, starting with all particles in state A and evolving to equilibrium, one can quickly see the effect the low barrier to isomerization has on the equilibrium distribution of states. For state A, the molecules can leave in two directions due to the periodic nature of the potential, and molecules can react into state A from each of the two nearest neighbors as well, seen in matrix form as:

$$\begin{pmatrix} -2k & k & 0 & 0 & 0 & k \\ k & -2k & k & 0 & 0 & 0 \\ 0 & k & -2k & k & 0 & 0 \\ 0 & 0 & k & -2k & k & 0 \\ 0 & 0 & 0 & k & -2k & k \\ k & 0 & 0 & 0 & k & -2k \end{pmatrix} \quad (6)$$

The reaction rate k describes the staggered to staggered transformation through the eclipsed state, treated as a transition state because of the low barrier calculated using DFT. The reaction kinetics for state A can be broken into three main exponential terms: the decay of molecules in state A, the growth into nearest neighbors, and the growth into two-well neighbors.

Chapter 3. Results and Discussion

3.1: BCT Structure

Initial characterization of the normal modes of the BCT carbonyl stretching frequencies was done using FTIR. The linear spectrum (**Fig. 6**) shows two main peaks, at 1980cm-1 and 1915cm-1 in hexane. The lower energy peak corresponds to two asymmetric modes, an Eg' and a T1u", while the higher energy peak is a single A1g symmetric stretch[23].

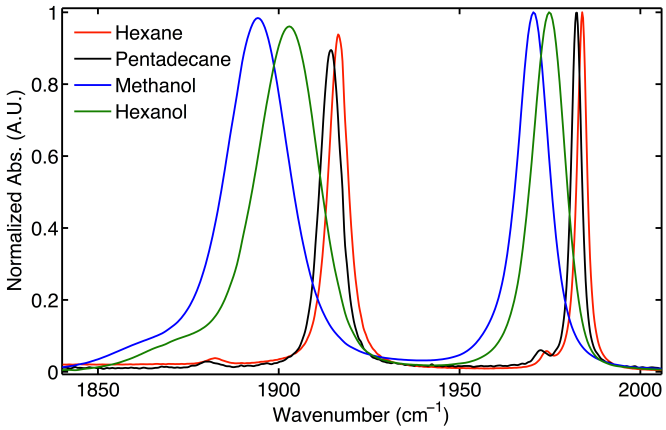

Figure 6: The FTIR spectra for BCT in a variety of solvents. The broadening in the polar solvents can be attributed to the complex fluctuating electric field that creates more microstates for the vibrational mode.

The symmetric stretch being isolated is of considerable interest to us for spectroscopic purposes, since any change in the symmetric stretch corresponds to some sort of environment change, not chemical exchange with another vibrational mode. Some general trends can be seen from the FTIR spectra of BCT; for one there is a red shift with increasing polarity of the solvent. However, the shifting of the vibrational peak frequency does not provide as much insight into the underlying chemical environments as the inhomogeneous broadening of the band. Measuring the full width at half maximum (FWHM) of a peak and seeing how it varies with a solvent series can

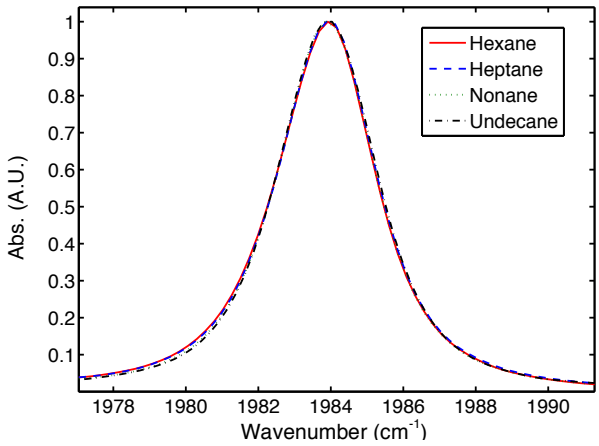

Figure 7: The FTIR spectra for BCT in a series of increasing chain length linear alkane solvents. Adjusting the peak maximum and normalizing, there is no change in the FWHM.

give insight into the rate at which different environments are sampled. In general, solvents that have a permanent dipole, such as alcohols, create multiple different solvent environments broadening the individual bands far more than alkane solvents, which lack a permanent dipole moment. It has been seen in some studies[18] that the viscosity increase from increasing chain length alcohol solvents causes longer spectral diffusion times. A good analogy for this effect is trying to swim in water versus swimming in molasses. The more viscous molasses provides considerably more resistance to motion and as such one can probably not swim as fast. **Fig. 7** shows a series of alkane solvents normalized and adjusted so they have the same maximum; it is clear that the increasing chain length alkane solvents do not change the FWHM of the peak.

To determine the stability of the metal carbonyl bond, a photodissociation study was done on BCT in hexane. As shown in **Fig. 8**, after a period of 5 minutes, the signal from the carbonyl vibrational modes has decayed roughly to zero. The carbonyls are more stable bound to the metal than free in solution, and as such we see rebinding of the carbonyl ligands after a similar period of time. For systems where the UV-radiation needed to dissociate the carbonyls does not cause damage, providing an interesting way to study the solvent at an interface or cavity by looking at the relative rebinding times of the carbonyl ligands. It also can provide information about the conformation of BCT in an inclusion complex.

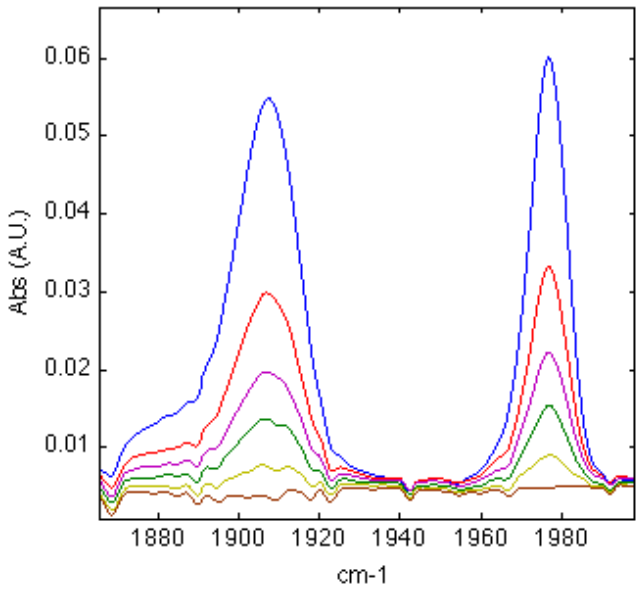

Figure 8: The photobleaching of BCT dissociates the carbonyl ligands and signal is lost from those vibrational modes. Each consecutive line represents an additional 1min of irradiation, with the blue curve at time zero.

3.2: BCT, A Molecular Rotor

Tripodal, piano-stool complexes are model systems for studying molecular rotors due to their small size, simplicity, and ability to undergo rotation about an arene-metal bond[4,5,28]. Early NMR studies of BCT and its analogues investigated the effect of bulky side chains intended to slow motion along the torsional reaction coordinate. Debates regarding the nature of restricted rotation about the arene-chromium bond initiated the study of torsional motion in BCT[29-31]. A later study combining high-field NMR for dynamics with x-ray crystallography for structure settled the debate by finding "unequivocal proof" of a slowed torsional reaction coordinate[9]. The study found that bulky side chains could slow the tripodal rotation, but did not investigate unsubstituted BCT since the rotation takes place faster than the NMR time scale. Experimental studies of BCT and the debate regarding the rotation about the arene-metal bond and structure of the molecule have been reviewed[32].

As computing power has continued to increase, studies have shifted to trying to define the reaction coordinate of BCT and its analogues using quantum chemistry. Multiple density functional theory studies have been conducted on BCT to determine the structure of the molecule using a variety of methods[23,33,34]. One study found that DFT optimized the structure of BCT better than Møller–Plesset second-order calculations (MP2) by comparing the bond lengths and angles to microwave data[33]. A later study of BCT using DFT calculations with higher level basis sets optimized the two stable isomers and found they were separated by a barrier roughly half of $k_B T$[34]. The study did not create a potential surface for the torsional coordinate or investigate solvent interactions on the torsional frequencies, both of which are considered here.

Most ultrafast studies of equilibrium reacting species in the recent literature have been carried out for systems that may be classified as examples of "slow exchange." In these cases, equilibrium chemical exchange can be monitored using 2D-IR spectroscopy by measuring the cross peak volumes, taking care to eliminate other competing dynamical phenomena such as orientational relaxation and intramolecular vibrational redistribution. Temperature dependent 2D-IR has been used to attempt to identify chemical exchange in an iron tricarbonyl system[35]. In this study, the authors conclude that the rate of intramolecular vibrational redistribution (IVR) is the principal mode of vibrational transfer and do not directly see chemical exchange. In a recent study of a torsionally isomerizing molecule, the rate of exchange was extracted from linear IR and Raman spectra over a range of temperatures. At increasing temperature, the two peaks broaden and overlap giving information about the rate of chemical exchange, which can be extracted from Voigt line shape analysis[36]. However, this method is not amenable to BCT due to the cooling requirements necessary to see the individual species split due to the much lower barrier of isomerization compared to the torsional reaction barrier for the iron tricarbonyl

molecule observed in the study. As is discussed in detail below, the torsional motion of BCT is a peculiar case of a system that might be considered to be an example of the "spectral diffusion" limit of chemical exchange. That is, changes in internal geometry induce spectral changes, but due to the very low (~k_BT/2) energy difference between isomers, there is nearly a continuous distribution of torsional bond angles populated at room temperature. Since we study the torsional dynamics exclusively in nonpolar solvents, using a vibrational band of BCT that is known to exhibit essentially no inhomogeneous broadening even in polar solvents, we are confident that the spectral fluctuations arise exclusively from internal torsional dynamics.

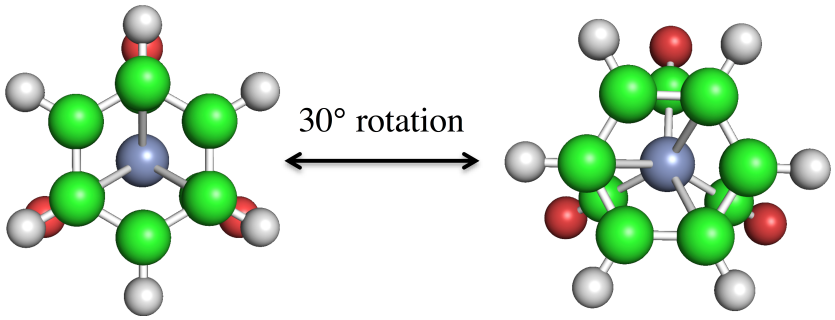

Figure 9: The torsional reaction coordinate of BCT is a low energy barrier rotation of the benzene with respect to the carbonyl ligands.

The reaction dynamics of BCT were studied and defined as the torsional motion of the benzene ring with respect to the tricarbonyl portion of the molecule (**Fig. 9**). The potential energy surface was calculated using DFT and the carbonyl vibrational frequencies extracted for the two stable conformations, staggered and eclipsed, along the reaction coordinate. The calculated barrier to isomerization is significantly less than k_BT, suggesting that interconversion between the two states occurs on ultrafast timescales, on the order of picoseconds. The slight ~2 cm^{-1} difference in the probed symmetric CO stretching mode is comparable to the homogeneous line width, placing the reaction dynamics in a regime that straddles chemical exchange and spectral diffusion. Using a recently introduced variation of heterodyne detected photon echo

spectroscopy called RASD[19], the diffusive reaction dynamics of BCT were monitored indirectly via the decay of the frequency fluctuation correlation function (FFCF), a key observable of IR photon echo spectroscopy. Similar to a previous work from the Kubarych Group on flexible metal carbonyl complexes, where we observed solvent friction retardation of barrier crossings in accord with Kramers' theory, here we also examine the solvent dependence of the torsional diffusive dynamics[18]. In striking contrast to that earlier work, we found there to be no variation of reaction time with alkane chain length. We interpret these results from the perspective of a solvent cage, where the dynamics of the solvent are independent of the diffusive torsional motion within the cavity. These results highlight key qualitative differences between macroscopic and nanoscopic machine components. When the size of the nano-component approaches that of the solvent, the traditional macroscopic view of friction has to be reassessed.

From the optimized BCT structures, the potential energy surface was calculated producing a periodic potential function corresponding to the torsional reaction coordinate. The reaction coordinate is one-dimensional, with torsional motion around the metal-benzene bond representing the only variable. From x-ray crystallography[37], BCT was found to have the asymmetric C_{3v} point group due to the non-planar benzene ring. However, the asymmetry is small compared to the effect of the torsional motion so a C_{6v} point group can be used as a good approximation when creating a periodic potential function for BCT.

The surface is characterized by a double-well potential, with the staggered and eclipsed conformers as stable states (**Fig. 10**). The global minimum staggered state is lower in energy than the eclipsed state by 0.28 kcal/mol, roughly half of k_BT, and is separated by a small reaction barrier roughly one thirtieth of k_BT, making it essentially diffusive relative to the eclipsed conformation. Due to the low barrier nature of the transition between staggered and eclipsed, the

interconversion between species is expected to occur rapidly at room temperature. For the purpose of kinetic studies used to calculate the reaction rate, the eclipsed state may be considered to be largely indistinguishable from a transition state due to it having a barrier roughly thirty times smaller than the staggered-to-eclipsed reaction.

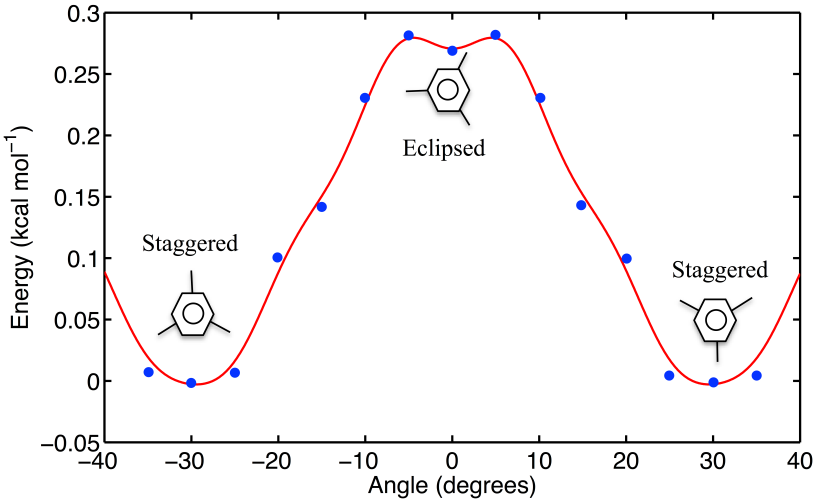

Figure 10: A periodic potential function (red) can be used to depict the internal rotation reaction coordinate of BCT. The two stable conformations of BCT are shown as cartoons. In blue, the approximation that the eclipsed conformer is a transition state.

Frequency calculations of the symmetric stretch of the staggered and eclipsed isomers exhibit a 2.1 cm^{-1} redshift when moving from staggered (1977.4 cm^{-1}) to eclipsed (1979.5 cm^{-1}), which provides the spectroscopic encoding of the torsional motion. Molecular volumes of the two states showed a difference of only 2%, 215 $Å^3$ and 210 $Å^3$ for the staggered and eclipsed isomers, respectively. For both the staggered and eclipsed isomers, the frequency calculations yielded only positive frequencies, implying that the two states are minima, since they have been optimized with respect to all degrees of freedom. Comparison with energy values along the reaction coordinate allows us to designate the staggered isomer as a global minimum and the eclipsed as a local minimum. Because of the low barrier from the eclipsed to staggered conformation, the eclipsed state is essentially a transition state. The small energy difference

between isomers implies that virtually every torsional angle is populated to some extent at room temperature. We revisit this angle distribution more quantitatively in the discussion below.

When investigating solvent dependent ultrafast kinetics, it is important to verify that the solvent does not trivially alter the reaction energetics. Since metal carbonyl complexes interact very weakly with nonpolar solvents, it is not expected that changing chain length will have a significant impact on the reaction barrier or the torsional mode frequency. Nevertheless, we verified this solvent independence by using a polarizable continuum solvation model to compute frequencies at the global minimum with increasing length linear alkanes selected from those used in the RASD experiments. For low frequency vibrations, our choice of basis and functional has been shown to need only a 1% correction factor[38], which is negligible compared to the vibrations themselves. The frequency of the torsional motion frequency in vacuum, 23.3 cm^{-1}, is slightly larger than that found using continuum models for hexane, nonane, dodecane and pentadecane (22.6 cm^{-1}, 22.7 cm^{-1}, 22.8 cm^{-1}, 22.8 cm^{-1} respectively). The invariance of the torsional mode frequency to different polarizable continuum modeled solvents demonstrates that the potential surface for the linear alkanes of interest is independent of solvent.

As seen in the FTIR for the linear alkane series, there is no difference in the full width at half maximum suggesting no change in inhomogeneous broadening. We emphasize the symmetric band, which is the one that is probed in the ultrafast spectral diffusion measurements for the torsional reaction. Fitting the bands to single Lorenztian functions yields 2.6 cm^{-1} widths that are indistinguishable relative to the fit error bars, and band centers that decrease slightly (~1 cm^{-1}) with increased alkyl chain length in an approximately linear fashion. These bands are among the narrowest the Kubarych group has observed in the course of many studies of transition metal carbonyl complexes in nonpolar solution. It is worth noting here that the most

symmetric bands of transition metal carbonyl complexes having more than two carbonyl units appear to exhibit idiosyncratic line narrowing. In many published examples, including our detailed investigation of $Mn_2(CO)_{10}$, it has been noted that the highest frequency IR active mode resists inhomogeneous broadening, even in polar solvents. In a nonpolar solvent environment presented by the alkane series, we would not expect to observe inhomogeneous broadening or spectral diffusion due solely to solvation dynamics. Any decay in the frequency fluctuation correlation function could therefore be attributed to some sort of internal process such as chemical exchange. Since the reaction barrier is so low, it is possible that a solvent-dependent

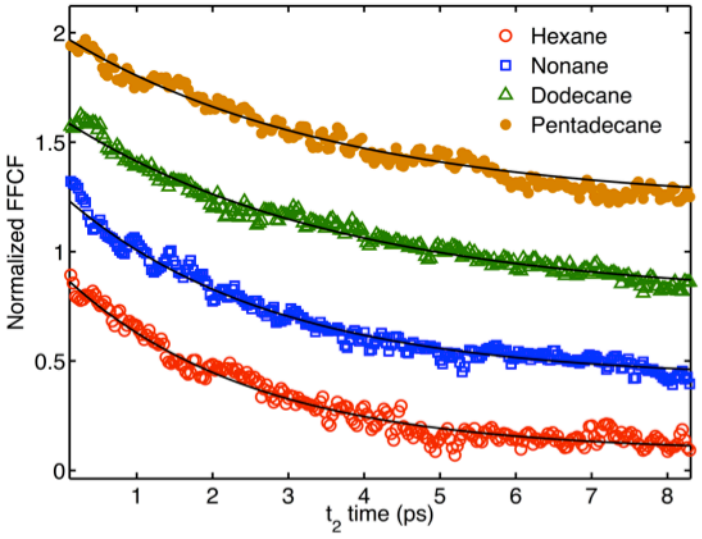

Figure 11: The normalized FFCF for each solvent is shown, offset by 0.4 and showing every fourth point for clarity. BCT spectral diffusion is independent of solvent viscosity over the linear alkane series.

effect is not noticeable in the FTIR spectra. The rate of exchange between the two isomers is so fast that even if it was solvent dependent, it's possible that the effect would be too small to observe.

To uncover the underlying dynamics of the system, we use RASD, a variation of 2DIR spectroscopy that can be utilized to quickly obtain the frequency-fluctuation correlation function. Due to the large number of data points that can be collected, the method is ideal for averaging

which can help minimize the signal to noise problems that typically plague 2D experiments. The FFCF for linear alkane solvents shows a clear independence of solvent viscosity, shown in **Fig. 11**. The spectral diffusion timescale, found by fitting the decay to a single exponential and extracting the time constant, is roughly 3 ps for all solvents within the fitting error.

The independence of spectral diffusion to alkane length defies the expected trend seen in previous work where increases in viscosity correspond to increases in the spectral diffusion time[18,15], or to increases in equilibrium reaction rate constants[3]. A viscosity dependent model suggests that the timescale of interconversion between isomers can be altered by solvent interactions; a more viscous solvent should induce recrossings of the dividing surface, ultimately leading to longer spectral diffusion times. In contrast to the solvent dependent Kramers model observed in a previous study[18], moving from hexane (0.3 cP) to pentadecane (3.8 cP) there is no detectable change in the spectral diffusion time. This leads to the conclusion that the solvent motion is completely decoupled from the internal torsional motion of the molecule.

The DFT results suggest a possible explanation for the solvent independence as arising from a solvent cage whose geometry need not be significantly altered to accommodate the torsional motion. The small, 2% change in molecular volume indicates there is little change in solvent packing in response to the torsional motion[3], suggesting that the solvent is not directly influencing the torsional motion. Changes in solvent-accessible surface area (~1%) are even smaller than molecular volume, further suggesting a weak influence of the solvent on the torsional motion. Because BCT is a small molecule, it is possible the linear alkane solvents are hindered by steric interactions and cannot pack close enough to the rotating benzene to damp the torsional motion differently based on chain length alone.

The difficulty in using 2DIR spectroscopy as a proxy for a reaction coordinate is that the measured values are frequencies, but in general the reaction coordinate of interest is defined by a spatial coordinates. Linking the frequency observed to the angle along the reaction coordinate is in general not trivial. Because non-stable states do not correspond to harmonic potential regions, any frequency obtained using DFT for a non-optimized structure will be of limited reliability. That means that accurate frequencies can only be computed for the staggered and eclipsed conformers. They show a splitting of 2.1 cm^{-1}, but how they vary in between the two stable states is not apparent. Modeling techniques are necessary to try to derive the relationship; unfortunately, the classical Langevin-type simulations that are fast and easy to test different frequency-position mappings do not apply to the BCT system, as it is solvent independent. There is no frictional term opposing the motion, since the solvent molecules form a solvent cage. However, the lack of solvent dependence can be further explained by looking at the phenomenological rate at which one population evolves into another using a six-state kinetic model.

The reaction kinetics for evolution from all molecules being in one of the six states (i.e. the survival probability), state A, can be broken into three main exponential terms: the decay of molecules leaving state A, the growth into nearest neighbors, and the growth into two-well neighbors (**Fig. 12**). The solution of interest is the decay of the initial population of molecules in A, which is a proxy for the spectral diffusion we observe as an initially excited state evolves to other states. However, this misses the kinetic contribution of neighbor states back into state A. The three exponential terms describing *P(A)*, the survival probability of remaining in initial state A, may be rearranged into a single exponential and two hyperbolic cosine functions of the form:

$$P(A) = \frac{1}{3}e^{-2kt}(2\cosh(kt) + \cosh(2kt)) \qquad (7)$$

Where the exponential term is the equilibrium rate of the molecules entering and leaving well A, with the hyperbolic term stretching the exponential at longer times and correcting the initial offset value to one. The exact physical interpretation of these hyperbolic functions is likely an artifact of the symmetry of the potential. It is possible that because of the symmetry, the growth rates from the nearest neighbor and second-nearest neighbor wells average out with the rate of decay from the main well. We find therefore that any time constant observed by us in an experiment will be a factor of two too slow compared to the actual reaction rate constant,

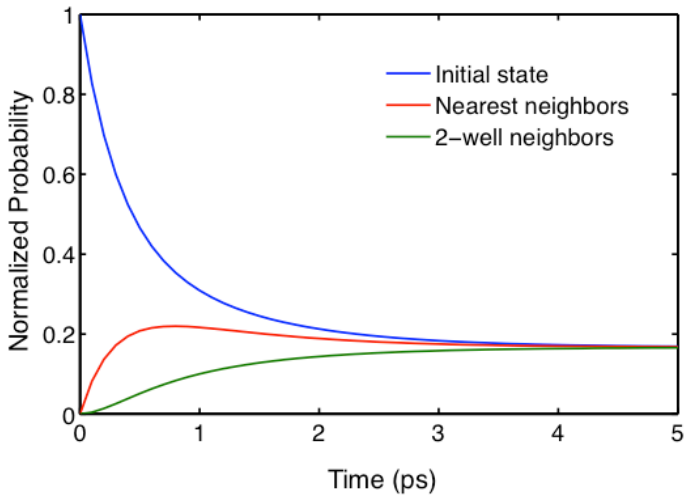

Figure 12: The evolution of BCT according to a six-state kinetic model where all particles start in one well (left). The blue curve corresponds to the loss from state A, while the red and yellow correspond to growth into nearest neighbors and next-nearest neighbor wells, respectively. For BCT, because the timescale of the torsional motion is fast, the single exponential term accurately fits the data.

notwithstanding additional modifications due to the mapping between structure and frequency. The result is exactly what would be the case for a two-state kinetic model; future work is needed to determine if this result holds for different barrier conditions and periodic potentials with more or fewer wells. The data shown in **Fig. 11** is fitted accurately using only a single exponential term; at longer timescales the hyperbolic terms skew the decay of the FFCF, but at short timescales the exponential term dominates. Since the timescale of internal rotation is so fast, we don't observe the hyperbolic terms because the FFCF approaches zero too quickly.

3.3 Biological and Biochemical Applications

3.3.1: Complexation with Cyclodextrin

In biological systems, regions around proteins and membranes have varying degrees of hydrophobicity[39]. To determine the properties and orientation of BCT in biological systems, we use β-cyclodextrin, a good model of a hydrophobic cavity with a hydrophilic exterior. BCT and β-cyclodextrin form a complex that is soluble in slightly polar solvents. Due to extensive washing and filtering, it is unlikely that any appreciable amount of the uncomplexed BCT is present, as BCT is soluble in water and the inclusion complex is not. The FTIR spectrum (**Fig. 13**) shows a splitting of the symmetric stretch into two clear peaks, one roughly in the same position as pure BCT and shifted 30cm^{-1} lower. In addition the broad lower frequency band is broadened as well compared to the pure BCT, meaning that it is likely that more environments exist for the carbonyls. Knowing that the carbonyl ligands are sensitive to UV-radiation, transient FTIR can be used to determine whether the ligands are constrained in a cavity or not, giving insight into the orientation of BCT. Interestingly, over a period of ten minutes of irradiation, the lower frequency band from the symmetric stretch resists change, while the higher frequency band decays to zero signal (**Fig. 14**).

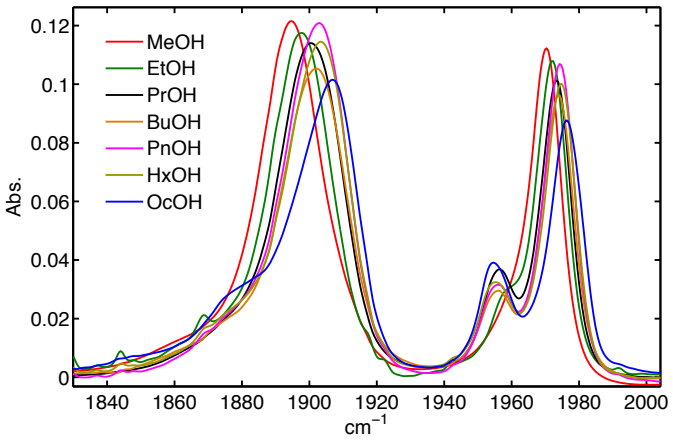

Figure 13: The BCT-cyclodextrin spectrum in various alcohol solvents is shown. The higher energy symmetric stretch splits into two distinct bands.

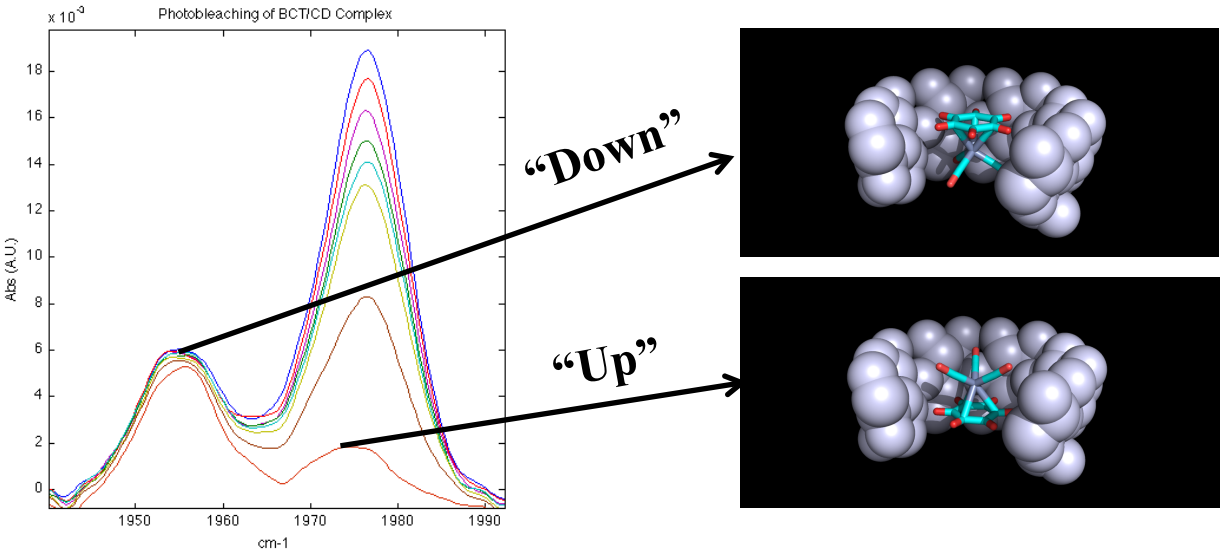

Figure 14: The transient FTIR spectra of photobleached BCT shows a clear decay of one band, corresponding to the "up" conformer and a near constant absorption of the other band corresponding to the "down" conformer. The difference in signal decay can be explained using geminate rebinding timescales. Each successive colored line in the overlay spectra (left) represents one minute of exposure to the UV light source.

It is therefore postulated that there are two conformations of the BCT-cyclodextrin complex: one with the carbonyl ligands pointed up out of the cavity, and another where they point down into the cavity. Rebinding time for the "down" conformer is faster than the acquisition time of the FTIR spectrometer, so a signal loss of the corresponding band does not occur. In contrast, the higher frequency band corresponding to the "up" isomer loses signal rapidly and has a rebinding time on the order of minutes. Even if some uncomplexed BCT is left in the sample and accounts for the higher frequency band, the splitting into two bands and resistance to UV-radiation is clearly caused by a complex with the cyclodextrin. There simply could not be enough change in the environment of pure BCT without interacting with some other molecule to cause that significant a shift in the frequency of the symmetric stretch. A previous study using cyclopentadienyl manganese tricarbonyl did not see this clear conformational difference[40], even though structurally the two molecules are similar with the exception that the cyclopentadienyl molecule has lower symmetry than benzene.

What is also interesting is the ratio of the "up" conformer to the "down" based on integrating the area of the two higher frequency symmetric peaks. Clearly, there is more "up" conformer, which makes sense based on the fact that the benzene is more likely to enter the hydrophobic core of the cyclodextrin than the fairly polar carbonyl ligands. Benzene is generally considered nonpolar due to the high symmetry of the molecule. However, due to pi-electron delocalization the molecule is miscible in small quantities in water and explains why it has some propensity to point away from the hydrophobic cyclodextrin core. Because the complexation reaction is sterically hindered in the sense that the cavity is not much larger than BCT, obtaining

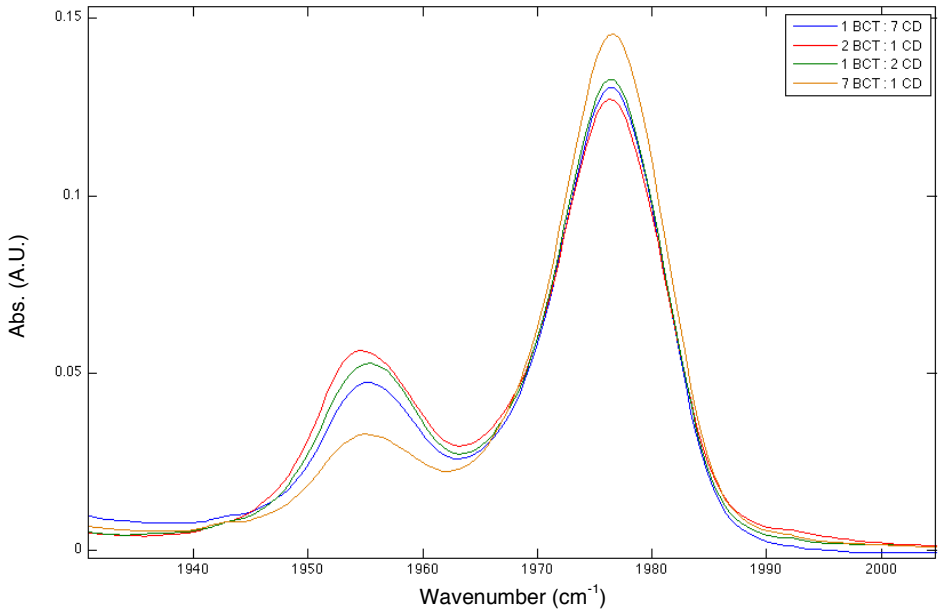

Figure 15: Varying the concentration of BCT and cyclodextrin has minimal effect on the abundance of the up and down conformers.

a high yield requires long reaction times to find the complex. Varying the mole ratio of BCT to cyclodextrin does not appear to change the ratio of the isomers significantly (**Fig. 15**). With a high excess of BCT, there is less down conformer; this complex may be less stable, as discussed based on the relative polarity of the benzene and carbonyl ligands. There are more BCT ligands present to interact with the cyclodextrin and find the most favorable conformation during the reaction. However, after a 1:2 ratio of BCT to cyclodextrin it appears that there is no longer any

trend in increasing the "down" conformer. It is possible that there is a limit for the amount of "down" conformer present. Initially, there are fewer BCT than cyclodextrin molecules and as such fewer interactions meaning that the more favorable "up" conformer is not sampled as often. Eventually, this effect saturates when there are not enough BCTs to fill all of the cyclodextrin cavities. It appears that the two conformers can not be isolated based on the synthesis conditions; a much more effective way to select the "down" conformer is to just photodissociate the "up" conformer so only the "down" remains with bonded carbonyl ligands. Of course, one has to be careful using this strategy as the carbonyls will rebind in a matter of minutes. Furthermore, a procedure to quench the free carbonyls allows for the interesting possibility of using of BCT as a carbon monoxide sensor.

3.3.2: BCT and Reverse Micelles

The Kubarych Lab has looked at BCT localized in a bicelle lipid layer by coupling it to cholesterol and found distinct differences between the bulk and the constrained water[41]. However, that study focused on the external polar solvent surrounding the bicelle, not a constrained water bath as described here for reverse micelles. The functionality of BCT, including the ability to dissociate the carbonyl ligands and measure the diffusive properties of the constrained water directly, makes it a logical next step in the progression to understanding molecular dynamics of constrained solvents in a small cavity.

AOT is a commonly used surfactant for the creation of reverse micelles with a negatively charged head group that protrudes into the water cavity[12]. BCT on its own is a small molecule relative to the micelle size, so it probably would be difficult to localize in the micelle cavity in order to study constrained water without being complex to another molecule. Cholesterol is

similar to the structure of AOT in that they both have large nonpolar regions; in theory adding BCT would act as a somewhat polar head group and the hydrophobic portion of cholesterol would point out into the bulk organic phase. BCT on its own shows fairly strong solubility for alcohol and alkane solvents and less of a preference for water.

Reverse micelles have been reviewed[42] and while the water cavity has been previously studied[43], a direct molecular probe of the water-micelle interface has to our knowledge not been used due to the difficulty getting inclusion in the membrane. One extremely important quantity for micelle studies is the equilibrium constant for inclusion, K[42] where:

$$K = \frac{[S_M]}{[S_B][M]} \qquad (8)$$

S_M is the solute concentration in the micelle, S_B is the solute concentration in the bulk organic phase, and M is the micelle concentration. What is important to note about the relation is that K does not give any information about how or where in the micelle the solute is located just that it is somehow forming a complex. However, based on K for cholesterol[44] while the majority of the cholesterol will prefer to be in the bulk organic phase, some will interact with the micelle. Again, this does not necessarily mean that the probe attached to cholesterol will be directed into the water cavity. Another important control on the system is the radius of the micelle based on w_0, which was measured and confirmed using DLS. For w_0 values of 5, 10 and 15 DLS determined an average radius of 1.77, 2.14, and 2.34nm, respectively. In the scattering profile there were two decays with vastly different timescales; this is suggestive of micelles aggregating in the solution.

If the BCT probe were located in the water cavity bound to the membrane by the cholesterol, we would expect a significant shift in the infrared spectrum, as the spectrum of BCT in bulk organic phase is different than that of BCT constrained near water due to the different

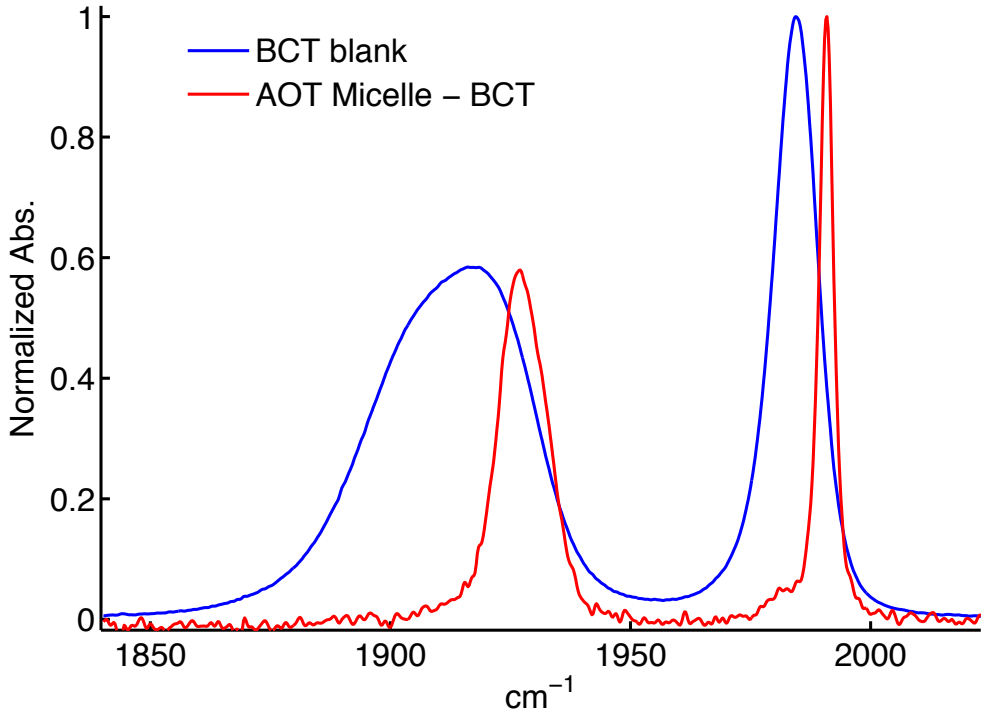

Figure 16: The FTIR spectrum for BCT-cholesterol in AOT micelles is narrowed from the bulk isooctane spectrum, but the wavelength shift and overall spectrum does not indicate incorporation in the micelle.

electronic environment. However, even over a range of concentrations of BCT-cholesterol in the water roughly mimicking a previous study for inclusion of a protein in reverse micelles[12], there is no difference between the BCT in bulk phase and BCT micelle spectra (**Fig. 16**). The lack of a vibrational frequency shift seems to suggest that the BCT-cholesterol has an overwhelming preference for the organic phase. Varying the size of the micelles using the w_0 ratio does not lead to any noticeable affect on the spectra; it is unlikely that the cholesterol is not incorporated into the monolayer because of sterics. Rather, it is likely that purely thermodynamic stability causes the cholesterol to stay in the organic phase. From a solubility point of view this seems to make some sense, since the cholesterol-BCT is dissolved initially in water, which is added to the

micelle solution dissolved in the organic solvent. The AOT self-assembles around the clusters of water while the BCT-cholesterol preferentially moves into the organic phase. If there were no thermodynamic driving force, the BCT-cholesterol would remain in the aqueous phase and the infrared spectrum of the carbonyls would reflect the constrained, polar environment. As it does not, it is safe to assume that BCT-cholesterol is not a suitable way to study the AOT reverse micelle polar cavity. Possible other approaches include using BCT with a slightly more polar group to try to facilitate the inclusion in the micelle. However, any carboxylic acid functionalized BCT would be negatively charged at the neutral pH used in these studies. Unfortunately, AOT head groups are also negatively charged which means that charge repulsion would push the BCT-acid derivative away from the micelle/water interface. At this point, the constrained water could be studied, but not the micelle interface with the water, which is of principle interest to the group. It is clear that another direction is probably needed than BCT for micelle studies.

3.3.3: NaSCN and Reverse Micelles

Since the ultimate goal of characterizing the location of a probe in a micelle system is to do 2DIR studies, it is worth looking at other molecules that have vibrational modes in the "clear window" of the infrared spectrum. The thiocyanate vibrational stretching mode has been fairly commonly used in 2DIR experiments in the past[45,46], making it a suitable molecule for study. Most importantly, thiocyanate is a negatively charged ion. While AOT reverse micelles contain negatively charged head groups, there are reverse micelles that can be synthesized with positive head groups, such as ammonium. This means that there is an electrostatic attraction causing the thiocyanate probe to spend more time near the positively charged water-micelle interface.

Finally, as an ionic species, thiocyanate is far more soluble in the aqueous phase than the organic phase so there is less of a preference for the thiocyanate to move between the phases.

Long chain alkanes terminated by an ammonium head group with a halide counter ion can be used to create reverse micelles. Interestingly, these ammonium halide surfactants have a built-in control like AOT on the micelle size; however, in this case it is relatively independent of the concentration of the aqueous and organic phases. For DTAB, TTAB, and CTAB, which each increase in alkane chain length, the measured average micelle radius increases as well from about 1.5nm to almost 3nm[47] depending on how the radius is determined.

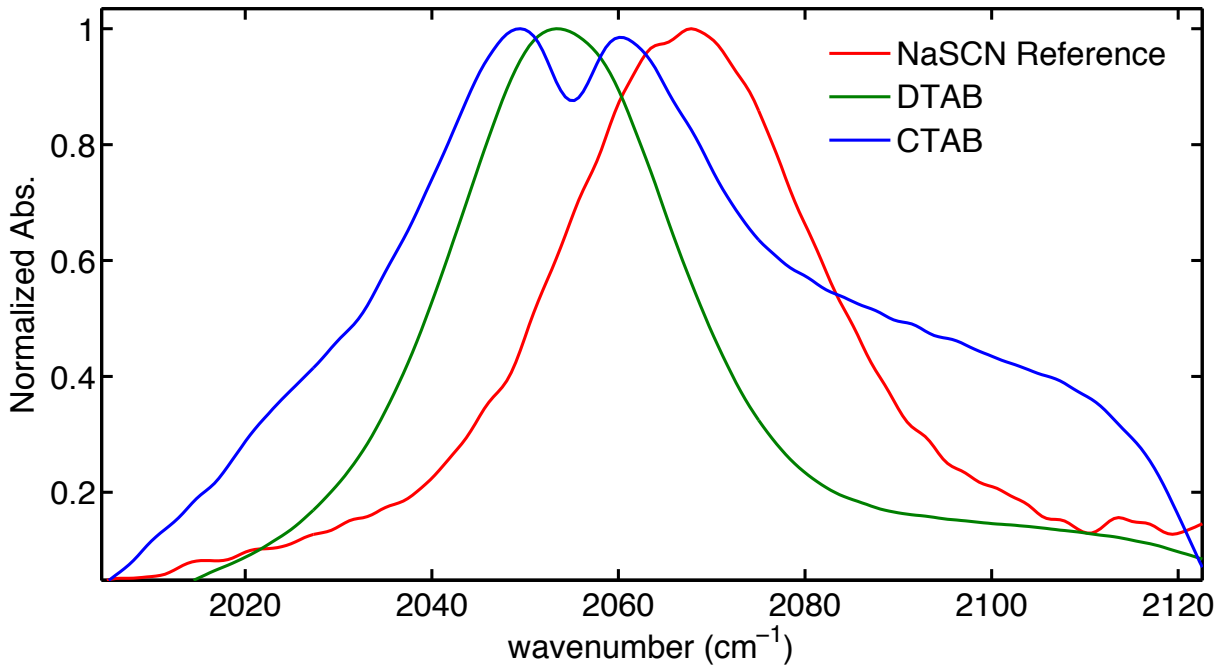

Figure 17: The FTIR spectrum for the cyanide band is shifted in DTAB, but clearly separated bands appear in CTAB indicative of multiple chemical environments.

The infrared spectrum of NaSCN has been studied previously in a crown ether complex[48] as well as in 2DIR studies of anionic clusters[49]. The CN stretching mode appears at roughly 2060cm^{-1} in aqueous solvents and shifts slightly depending on the chemical environment. A

comparison of the CN stretch in bulk DCM and in a solution of CTAB and DTAB micelles is shown in **Fig. 17**.

For DTAB, the CN stretch is shifted 20cm^{-1} to lower frequency, but shows no change in the FWHM. Isooctane and dichloromethane, used in all studies with micelles as the organic phase, could also shift the CN stretch when compared to an aqueous environment. However, as seen with BCT, generally the symmetric stretch shifts to higher frequency with a less polar solvent. That, in addition to the strong preference for the anion to remain in the aqueous phase on the basis of solubility leads to the conclusion that the SCN^- is interacting with the micelles and is not present only in the bulk organic phase. From this analysis, it is most probable that the SCN^- ions are in the aqueous micelle interior, due to the large shift in the vibrational frequency. However, because there is no appreciable change in the FWHM, it appears that SCN^- is not in multiple environments in the micelle, similar to what is seen for SCN^- in bulk aqueous solvent. Because the radius of the micelle is small, there may only be one environment or a steric issue with too many SCN molecules in the micelle. Based on the concentrations used, there is roughly 0.5mmols of DTAB in the solution corresponding to 11.7μmol of micelles based on using the average number of molecules in an aggregate[50]. The quantity of NaSCN in solution was varied over a range from 3 to 10μmol. Thus, it is most likely for a single SCN^- ion to sit in a micelle; this minimizes the effects of the ions interacting in the small aqueous cavity and also allows for the easier determination of the location of the ion. So, based on this analysis it is probable that since only a single thiocyanate is in a micelle on average that there is only one chemical environment that it spends most of its time in.

Contrast that with the spectra for the roughly double radius micelles formed by CTAB. There are clearly two peaks broadening the main CN stretch and a shoulder at a higher frequency

than the thiocyanate reference in DCM. The broadening could be due to some of the probes residing in the micelle monolayer potentially, or perhaps from some being in the organic phase. What is interesting is that the lower frequency band seen in the DTAB spectrum is now split into two species separated by 15cm^{-1}. Since the concentrations of the micelles and the NaSCN are on the same scale as for CTAB, it is now likely that due to the increased size of the micelle there are multiple environments that the probe spends substantial time in. It would make intuitive sense for this to mean that the aqueous phase is now large enough that the probe can be in a "bulk-like" region and an interfacial constrained region. This idea could be tested using the intermediately sized TTAB to see if it follows the trend seen here where the aqueous cavity enlarges to the point that the center is "bulk-like". If one of the bands is larger for TTAB than the seemingly equal area seen in the CTAB spectrum then it is likely that band is caused by different chemical environments in the aqueous phase.

3.3.4: Future Directions

Using CTAB, it appears that multiple chemical environments are present for the thiocyanate ion, which influences the vibrational frequency of the stretching mode. The electrostatic attraction of the probe to the head groups of the micelle could allow for easily studying the micelle-water interface directly. Further work is needed to determine the exact distribution of the locations the probe inhabits in the micelle. Varying the amount of thiocyanate molecules added so that they are in excess to the number of micelles in the system, varying the temperature, and changing the solvent properties could help unravel the different chemical environments. It is possible that with increasing thermal energy in the system the thiocyanate ions could sample the different environments in the micelle more rapidly as the electrostatic

attraction to the ammonium head groups is overcome by the increased internal energy. To determine if there is substantial electrostatic attraction to the ammonium head group, the pH of the solution can be varied. By protonating some of the thiocyanate ions (pKa ~1.1 so it is difficult to achieve full protonation), the negative-positive ion interaction would perhaps be partially quenched, as there is now only a positive-neutral interaction between the head group and the thiocyanate. If the signal for one of the bands in the CTAB spectrum decreases, this could certainly be one of the possible reasons. Using 2DIR spectroscopy, it may be possible to determine the timescales for switching from one environment, perhaps non-covalently interacting with the micelle interface, to another more bulk aqueous environment. If the timescale is slow enough, ultrafast spectroscopy might not even need to be used to determine the sampling rate. Ultimately, a model could be created to look at the mobility of small solutes in reverse micelles and their spatial distribution depending on factors like pH and temperature, with applications in drug delivery systems.

It is also worth noting that BCT with a carboxylic acid group could be used as a probe as well since its negative charge in neutral pH solutions mimics that of the thiocyanate ion. If a method can be found to incorporate BCT into the micelle membrane exclusively, then the carbonyl ligands can be dissociated using UV radiation and a study of the rebinding timescales can be used to look directly at the size of the micelle and the electronic environment of the constrained water. The timescale for rebinding could be used to estimate the distance travelled by the carbonyl ligand, giving rise to a sort of molecular “tape measurer” to determine the relative size of the micelle cavity. This sort of a controlled diffusive study could give new insight into the timescales of cellular level processes, which are often controlled by diffusion.

One ongoing investigation in the group involves determining why the higher frequency carbonyl symmetric stretch is more resistant to spectral diffusion than the lower frequency asymmetric stretches. Another graduate student has been studying the charge transfer bands of $Re(CO)_3(bpy)Cl$[51], abbreviated as ReCl. To determine if higher frequency modes in ReCl are less susceptible to coupling to the fluctuating electric medium that represents a solvent, DFT frequency calculations can be used with point charges. By choosing a variety of different configurations for the point charges placed on a sphere of a set radius from the center of the molecule and looking at the standard deviation of the frequencies for each mode, we can determine the susceptibility of modes to a charged environment that is constantly in flux. This approach seeks to deconstruct the solvent molecules into points of electric charge; averaging over a large number of configurations should give an accurate picture of how susceptible to electronic coupling each vibrational mode frequency is in a solvent environment. Some general technical difficulties exist with the implementation in Gaussian, the most important of which is the usage of Z-matrix coordinates. The Z-matrix coordinate system defines a dihedral angle between atoms as only from 0 to 180 degrees. If you have linear bonds like a carbonyl, the Z-matrix implantation often crashes. Crashing occurs because unless there is knowledge of which direction the bond will optimize in, it is easy to break the simulation with bond angles greater than 180º. This problem has been slightly overcome in recent simulations; we have collected enough preliminary data to say that it is indeed possible that the symmetric higher frequency stretch is coupled less strongly to the solvent fluctuations, but not enough to be analytically sure. Therefore, more computations need to be run to get more point charge configurations and a smaller chance that the results are in error.

Chapter 4. Conclusions

While widely used by organic chemists to determine the extent of a reaction based on the functional groups for compound identification, infrared spectroscopy is also heavily utilized by physical chemists to elucidate the dynamics of chemical systems. 2DIR is a commonly used tool to look at ultrafast timescales by examining how a vibrationally excited mode relaxes, through processes like intramolecular vibrational energy transfer and chemical exchange. Metal carbonyl compounds are excellent probes for 2DIR because the carbonyl vibrational stretching modes are intense and in the "clear window" of the infrared spectrum. Benzene chromium tricarbonyl (BCT) was characterized using FTIR and 2DIR spectroscopy and a number of interesting properties were investigated. First, the ability of the carbonyls to dissociate from the chromium metal upon excitation with UV radiation was studied with FTIR, finding that the carbonyls dissociate and rebind completely on a timescale of a few minutes. Using a new variant of 2DIR called "rapidly acquired spectral diffusion" or RASD, the internal torsional reaction coordinate of BCT that was studied by computational chemists was directly observed and found to occur on ultrafast single picosecond timescales. The torsional motion is characterized by the low barrier motion between two conformations of BCT, the "staggered" and "eclipsed" conformers. The periodic potential for the internal motion was mapped using DFT and was found to agree with the calculated values for the barrier to rotation in the literature. Directly probing the equilibrium motion of the essentially one-dimensional torsional reaction coordinate of BCT provides insight into some of the complications for design of a molecular nano-machine. Due to the solvent molecules being roughly the same size as the nano-motor components, the macroscopic model of friction breaks down. The solvent molecules are sterically hindered in their ability to damp the

motion of the rotor and form a "solvent cage" where the rotor is virtually unhindered by the solvent.

BCT was also used to investigate a variety of biologically relevant systems. Constrained water at protein interfaces behaves differently than the bulk water and transport properties may need to be modified to account for this difference. To determine whether BCT is an effective probe for these sorts of systems BCT was complexed with β-cyclodextrin, a simple model of a system containing a hydrophobic core and a hydrophilic exterior. Using the ability of UV radiation to dissociate the carbonyl ligands, the conformation of BCT in the cavity was able to be determined based on the rebinding times for the ligands. BCT sits in two conformations: an "up" and "down" conformer defined based on whether the carbonyl ligands are pointing out of, or into, the hydrophobic cavity, respectively. The ability to select different conformations through photodissociation of ligands could prove powerful for infrared studies of constrained water systems. For instance, a sample could be exposed to UV-radiation prior to a pump-probe or 2DIR experiment in order to study only the carbonyls pointing into a cavity (since they rebind on faster timescales).

Finally, the groundwork for 2D studies of both BCT and NaSCN as probes for studying reverse micelle systems has been laid. Electrostatic attraction and repulsion needs to be taken into account in order to facilitate the association of small probe molecules to the micelle-water interface. It is important to also consider the relative solubility of the probe in the two phases; significant exchange across the micelle membrane could make it difficult to study only the micelle-water interface and the properties of the aqueous cavity. An attempt to use a cholesterol-BCT complex to sit in the monolayer of AOT micelles with the BCT pointing into the aqueous phase was unsuccessful due to the strong preference for cholesterol to be located in the organic

phase. Using smaller, charged probes such as NaSCN and using oppositely charged micelle head groups proved more successful to localize the probes in the aqueous phase. Micelles are an ideal way to study the nature of constrained water, as size control of the micelle allows for the determination of the transition from constrained to "bulk-like" properties. The possibility to dissociate a carbonyl ligand and watch the timescale for rebinding could give new insight into the diffusive processes as they occur in cellular systems.

Chapter 5. Acknowledgements

There are a number of people without whom this work would not be possible. First and foremost, I would like to thank Professor Kubarych for all his mentorship and guidance over the last three years. I have been able to grow as a scientist and gain understanding and knowledge about chemistry and physics, but perhaps more importantly about life in general. I also wish to thank my graduate student mentor Dr. Derek Osborne, a recent graduate in biophysics. Derek was instrumental in helping me understand the practical implementation of the spectroscopic techniques the lab uses for BCT and his development of RASD led to the excellent data on the BCT internal reaction coordinate. I am thankful for Derek's guidance and patience with me as I tried (and failed) many attempts to get good data. I also wish to thank the entire rest of the Kubarych Group for their help with various aspects of physical and computational chemistry I could not have figured out on my own, especially to Aaron White for his knowledge of Density Functional Theory. Thank you to my friends, both old and new, for your support during the process of both researching and writing this thesis. I could not conclude this work without thanking my parents and family; the values you've instilled in me, including a love and appreciation of science, have made me into the person I am today.

Chapter 6. DFT Optimized Structures

Atom	X (Å)	Y (Å)	Z (Å)
C	-1.633514	1.193773	-0.759884
C	-1.632165	-0.051273	-1.414499
C	-1.631979	-1.256182	-0.654300
C	-1.631209	-1.200452	0.751347
C	-1.632948	0.060235	1.415002
C	-1.632776	1.249500	0.663793
H	-1.594251	2.111662	-1.337685
H	-1.592630	-0.095034	-2.498250
H	-1.591560	-2.215505	-1.160182
H	-1.591024	-2.117087	1.331087
H	-1.593096	0.101952	2.498769
H	-1.593961	2.210063	1.167637
Cr	0.108540	0.000080	0.000168
C	1.192459	-0.794286	-1.285245
C	1.193353	-0.715260	1.330590
C	1.191431	1.511215	-0.045787
O	1.842357	2.468407	-0.074941
O	1.845694	-1.168546	2.173057
O	1.843905	-1.297562	-2.099556

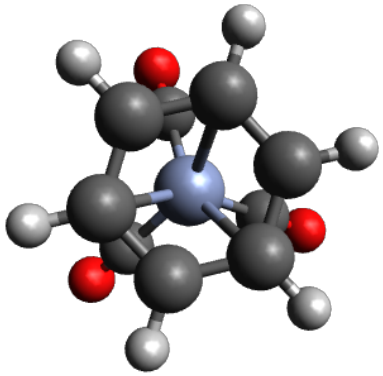

Staggered Isomer
Energy = -1616.7478 Hartrees

Atom	X (Å)	Y (Å)	Z (Å)
C	1.646534	-1.359415	0.416087
C	1.630801	-1.028416	-0.960196
C	1.647902	0.322515	-1.381703
C	1.627880	1.349345	-0.407477
C	1.642655	1.037857	0.973014
C	1.624183	-0.319300	1.375473
H	1.610657	-2.397004	0.730021
H	1.589098	-1.820273	-1.702291
H	1.613773	0.568589	-2.437512
H	1.584195	2.387765	-0.722073
H	1.605145	1.828759	1.714310
H	1.576894	-0.565567	2.432004
Cr	-0.108625	0.000245	-0.000698
C	-1.192792	-1.106026	-1.027424
C	-1.194803	1.441466	-0.445495
C	-1.198270	-0.336605	1.467486
O	-1.853880	-0.550537	2.397613

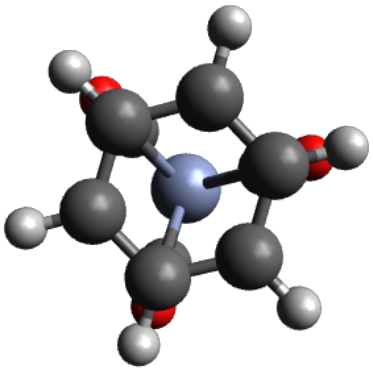

Eclipsed Isomer
Energy = -1616.7474 Hartrees

O	-1.848067	2.355323	-0.726221
O	-1.845217	-1.806870	-1.678430

Chapter 7. References

(1) King, J. T.; Arthur, E. J.; Brooks, C. L.; Kubarych, K. J. *The Journal of Physical Chemistry B* **2012**, *116*, 5604.

(2) Anna, J. M.; Ross, M. R.; Kubarych, K. J. *The Journal of Physical Chemistry A* **2009**, *113*, 6544.

(3) Anna, J. M.; King, J. T.; Kubarych, K. J. *Inorg. Chem. (Washington, DC, U. S.)* **2011**, *50*, 9273.

(4) Du Plooy, K. E.; Marais, C. F.; Carlton, L.; Hunter, R.; Boeyens, J. C. A.; Coville, N. J. *Inorganic Chemistry* **1989**, *28*, 3855.

(5) Eisenberg, A.; Shaver, A.; Tsutsui, T. *Journal of the American Chemical Society* **1980**, *102*, 1416.

(6) Conyard, J.; Addison, K.; Heisler, I. A.; Cnossen, A.; Browne, W. R.; Feringa, B. L.; Meech, S. R. *Nat. Chem.* **2012**, *4*, 547.

(7) Koumura, N.; Zijlstra, R. W.; van, D. R. A.; Harada, N.; Feringa, B. L. *Nature* **1999**, *401*, 152.

(8) Astumian, R. D. *Science* **1997**, *276*, 917.

(9) Downton, P. A.; Mailvaganam, B.; Frampton, C. S.; Sayer, B. G.; McGlinchey, M. J. *Journal of the American Chemical Society* **1990**, *112*, 27.

(10) Hagler, A. T.; Moult, J. *Nature* **1978**, *272*, 222.

(11) Song, L.-X.; Meng, Q.-J.; You, X.-Z. *Chinese Journal of Chemistry* **1995**, *13*, 311.

(12) Mukherjee, S.; Chowdhury, P.; DeGrado, W. F.; Gai, F. *Langmuir* **2007**, *23*, 11174.

(13) Boyd, J. E.; Briskman, A.; Sayes, C. M.; Mittleman, D.; Colvin, V. *The Journal of Physical Chemistry B* **2002**, *106*, 6346.

(14) Yokozeki, A.; Kasprzak, D. J.; Shiflett, M. B. *Applied Energy* **2007**, *84*, 863.

(15) King, J. T.; Baiz, C. R.; Kubarych, K. J. *The Journal of Physical Chemistry A* **2010**, *114*, 10590.

(16) Anna, J. M.; Nee, M. J.; Baiz, C. R.; McCanne, R.; Kubarych, K. J. *J. Opt. Soc. Am. B* **2010**, *27*, 382.

(17) Kwak, K.; Park, S.; Finkelstein, I. J.; Fayer, M. D. *The Journal of chemical physics* **2007**, *127*.

(18) Anna, J. M.; Kubarych, K. J. *J. Chem. Phys.* **2010**, *133*, 174506/1.

(19) Osborne, D. G.; Kubarych, K. J. *The Journal of Physical Chemistry A* **2012**.

(20) Roberts, S. T.; Loparo, J. J.; Tokmakoff, A. *J. Chem. Phys.* **2006**, *125*, 084502/1.

(21) Ogilvie, J. P.; Kubarych, K. J. In *Advances In Atomic, Molecular, and Optical Physics*; E. Arimondo, P. R. B., Lin, C. C., Eds.; Academic Press: 2009; Vol. Volume 57, p 249.

(22) Gaussian 03, Revision C.02,
M. J. Frisch, G. W. Trucks, H. B. Schlegel, G. E. Scuseria,
M. A. Robb, J. R. Cheeseman, J. A. Montgomery, Jr., T. Vreven,
K. N. Kudin, J. C. Burant, J. M. Millam, S. S. Iyengar, J. Tomasi,

V. Barone, B. Mennucci, M. Cossi, G. Scalmani, N. Rega,
G. A. Petersson, H. Nakatsuji, M. Hada, M. Ehara, K. Toyota,
R. Fukuda, J. Hasegawa, M. Ishida, T. Nakajima, Y. Honda, O. Kitao,
H. Nakai, M. Klene, X. Li, J. E. Knox, H. P. Hratchian, J. B. Cross,
C. Adamo, J. Jaramillo, R. Gomperts, R. E. Stratmann, O. Yazyev,
A. J. Austin, R. Cammi, C. Pomelli, J. W. Ochterski, P. Y. Ayala,
K. Morokuma, G. A. Voth, P. Salvador, J. J. Dannenberg,
V. G. Zakrzewski, S. Dapprich, A. D. Daniels, M. C. Strain,
O. Farkas, D. K. Malick, A. D. Rabuck, K. Raghavachari,
J. B. Foresman, J. V. Ortiz, Q. Cui, A. G. Baboul, S. Clifford,
J. Cioslowski, B. B. Stefanov, G. Liu, A. Liashenko, P. Piskorz,
I. Komaromi, R. L. Martin, D. J. Fox, T. Keith, M. A. Al-Laham,
C. Y. Peng, A. Nanayakkara, M. Challacombe, P. M. W. Gill,
B. Johnson, W. Chen, M. W. Wong, C. Gonzalez, and J. A. Pople,
Gaussian, Inc., Wallingford CT, 2004.

(23) Spears, K. G. *Journal of Physical Chemistry A* **1997**, *101*, 6273.

(24) Gaussian 09, Revision A.02,
M. J. Frisch, G. W. Trucks, H. B. Schlegel, G. E. Scuseria,
M. A. Robb, J. R. Cheeseman, G. Scalmani, V. Barone, B. Mennucci,
G. A. Petersson, H. Nakatsuji, M. Caricato, X. Li, H. P. Hratchian,
A. F. Izmaylov, J. Bloino, G. Zheng, J. L. Sonnenberg, M. Hada,
M. Ehara, K. Toyota, R. Fukuda, J. Hasegawa, M. Ishida, T. Nakajima,
Y. Honda, O. Kitao, H. Nakai, T. Vreven, J. A. Montgomery, Jr.,
J. E. Peralta, F. Ogliaro, M. Bearpark, J. J. Heyd, E. Brothers,
K. N. Kudin, V. N. Staroverov, R. Kobayashi, J. Normand,
K. Raghavachari, A. Rendell, J. C. Burant, S. S. Iyengar, J. Tomasi,
M. Cossi, N. Rega, J. M. Millam, M. Klene, J. E. Knox, J. B. Cross,
V. Bakken, C. Adamo, J. Jaramillo, R. Gomperts, R. E. Stratmann,
O. Yazyev, A. J. Austin, R. Cammi, C. Pomelli, J. W. Ochterski,
R. L. Martin, K. Morokuma, V. G. Zakrzewski, G. A. Voth,
P. Salvador, J. J. Dannenberg, S. Dapprich, A. D. Daniels,
O. Farkas, J. B. Foresman, J. V. Ortiz, J. Cioslowski,
and D. J. Fox, Gaussian, Inc., Wallingford CT, 2009.

(25) Levy, R. M.; Karplus, M.; McCammon, J. A. *Chemical Physics Letters* **1979**, *65*, 4.

(26) Dote, J.; Kivelson, D.; Schwartz, R. N. *Journal of Physical Chemistry* **1981**, *85*, 2169.

(27) Cleary, L.; Coffey, W. T.; Dowling, W. J.; Kalmykov, Y. P.; Titov, S. V. *Journal of Physics A: Mathematical and Theoretical* **2011**, *44*, 475001.

(28) Hansen, V. M.; Batchelor, R. J.; Einstein, F. W. B.; Male, J. L.; Pomeroy, R. K.; Zaworotko, M. J. *Organometallics* **1997**, *16*, 4875.

(29) Gracey, D. E. F.; Jackson, W. R.; Jennings, W. B.; Rennison, S. C.; Spratt, R. *Chem. Commun. (London)* **1966**, 231.

(30) Jackson, W. R.; Jennings, W. B.; Spratt, R. *Journal of the Chemical Society D: Chemical Communications* **1970**, 593.

(31) Jula, T. F.; Seyferth, D. *Inorg. Chem.* **1968**, *7*, 1245.

(32) McGlinchey, M. J. **1992**, *34*, 285.
(33) Low, A. A.; Hall, M. B. *International Journal of Quantum Chemistry* **2000**, *77*, 152.
(34) Gribanova, T. N.; Minyaev, R. M.; Starikov, A. G.; Minkin, V. I. *Russian Chemical Bulletin* **2009**, *58*, 691.
(35) Hill, A. D.; Zoerb, M. C.; Nguyen, S. C.; Lomont, J. P.; Bowring, M. A.; Harris, C. B. *The Journal of Physical Chemistry B* **2013**.
(36) Giordano, A. N.; Morton, S. M.; Jensen, L.; Lear, B. J. *The Journal of Physical Chemistry A* **2013**, *117*, 2067.
(37) Field, C. N.; Green, J. C.; Moody, A. G. J.; Siggel, M. R. F. *Chemical Physics* **1996**, *206*, 211.
(38) Andersson, M. P.; Uvdal, P. *J. Phys. Chem. A* **2005**, *109*, 2937.
(39) Nelson, D. L.; Lehninger, A. L.; Cox, M. M. *Lehninger Principles of Biochemistry*; W. H. Freeman, 2008.
(40) Osborne, D. G.; King, J. T.; Dunbar, J. A.; White, A. M.; Kubarych, K. J. *The Journal of chemical physics* **2013**, *138*.
(41) Osborne, D. G.; Dunbar, J. A.; Lapping, J. G.; White, A. M.; Kubarych, K. J. *The Journal of Physical Chemistry B* **2013**, *117*, 15407.
(42) Silber, J. J.; Biasutti, A.; Abuin, E.; Lissi, E. *Advances in Colloid and Interface Science* **1999**, *82*, 189.
(43) Costard, R.; Greve, C.; Heisler, I. A.; Elsaesser, T. *The Journal of Physical Chemistry Letters* **2012**, *3*, 3646.
(44) D'Aprano, A.; Donato, I. D.; Pinio, F.; Liveri, V. T. *J Solution Chem* **1990**, *19*, 1055.
(45) Park, S.; Ji, M.; Gaffney, K. J. *The Journal of Physical Chemistry B* **2010**, *114*, 6693.
(46) Baiz, C. R.; Kubarych, K. J. *Journal of the American Chemical Society* **2010**, *132*, 12784.
(47) Baar, C.; Buchner, R.; Kunz, W. *The Journal of Physical Chemistry B* **2001**, *105*, 2914.
(48) Xu, M.; Eyring, E. M.; Petrucci, S. *The Journal of Physical Chemistry* **1995**, *99*, 14589.
(49) Bian, H.; Wen, X.; Li, J.; Chen, H.; Han, S.; Sun, X.; Song, J.; Zhuang, W.; Zheng, J. *Proceedings of the National Academy of Sciences* **2011**.
(50) Tavernier, H. L.; Laine, F.; Fayer, M. D. *The Journal of Physical Chemistry A* **2001**, *105*, 8944.
(51) George, M. W.; Johnson, F. P. A.; Westwell, J. R.; Hodges, P. M.; Turner, J. J. *Journal of the Chemical Society, Dalton Transactions* **1993**, 2977.